Surface & Coatings Technology 327 (2017) 146–157

Contents lists available at ScienceDirect

Surface & Coatings Technology

journal homepage: www.elsevier.com/locate/surfcoat

Electrophoretic deposition of tetracycline hydrochloride loaded halloysite nanotubes chitosan/bioactive glass composite coatings for orthopedic implants

Namir S. Radda'a [a], Wolfgang H. Goldmann [b], Rainer Detsch [a], Judith A. Roether [c], Luis Cordero-Arias [d], Sannakaisa Virtanen [e], Tomasz Moskalewicz [f], Aldo R. Boccaccini [a,*]

[a] Institute of Biomaterials, Department of Materials Science and Engineering, University of Erlangen-Nuremberg, Cauerstrasse 6, 91058 Erlangen, Germany
[b] Biophysics group, Center for Medical Physics and Technology, University of Erlangen-Nuremberg, Henkestrasse 91, 91052 Erlangen, Germany
[c] Institute of Polymer Science, Department of Materials Science and Engineering, University of Erlangen-Nuremberg, Martensstr. 7, 91058 Erlangen, Germany
[d] Escuela de Ciencia e Ingeniería de los Materiales (ECIM), Costa Rican Institute of Technology (ITCR), Cartago 159-7050, Costa Rica
[e] Institute of Surface Science and Corrosion, Department of Materials Science and Engineering, University of Erlangen-Nuremberg, Martensstrasse 7, 91058 Erlangen, Germany
[f] Faculty of Metals Engineering and Industrial Computer Science, AGH University of Science and Technology, Czarnowiejska 66, 30-054 Kraków, Poland

ARTICLE INFO

Article history:
Received 19 March 2017
Revised 25 June 2017
Accepted in revised form 20 July 2017
Available online 21 July 2017

Keywords:
Electrophoretic deposition
Chitosan
Bioactive glass
Tetracycline hydrochloride
Halloysite nanotubes
Stainless steel
Antibacterial

ABSTRACT

Electrophoretic deposition (EPD) was used to apply bioactive multifunctional composite coatings with antibacterial substances on stainless steel AISI 316L (SS). Tetracycline hydrochloride (TCN) loaded halloysite nanotubes were co-deposited with chitosan and bioactive glass (BG) particles to produce composite coatings. SEM/EDX, XRD, and FTIR analyses were performed to characterize the composition and microstructure of coatings. The release of tetracycline hydrochloride (TCN) in phosphate buffered saline (PBS) was investigated by UV spectrometry, and measurements indicated the release of around 54% of the drug within 14 days of immersion in PBS. Furthermore, to determine that the bioactivity of coatings had not been adversely influenced, simulated body fluid (SBF) bioactivity tests were performed. The formation of hydroxyl carbonate apatite on the surface of the coatings was confirmed after 3 days. The ability of coatings to prevent bacterial growth was tested using *E. coli* as gram-negative and *S. aureus* as gram-positive bacteria. Results showed improved bactericidal effect of TCN-containing coatings compared to non-TCN loaded coatings. The corresponding amount of TCN loaded in EPD coatings supported cell viability and proliferation of MG-63 cells for up to 3 days. Fluorescence images of MG-63 cells showed evidence of cell growth in islands on the coated surface. The surface roughness of the coating loaded with halloysite nanotubes supported cell adhesion and proliferation. Additionally, the wettability value of the coatings confirmed a moderately hydrophilic surface, which is suitable for bone regenerative applications. Improved corrosion resistance compared to the pure stainless steel (SS) substrate was confirmed. The adhesion between coatings and substrates was tested by the tape test, and the result showed sufficient adhesion of the coatings to be handled without detachment. In all, the new coating system has potential for applications in orthopedics.

1. Introduction

One convenient method to produce coatings on metallic substrates is electrophoretic deposition (EPD) [1–3]. For attaining a uniform particle packing structure of electrophoretic deposits, adequate stabilization of suspensions is required; this depends on numerous factors including the amount of surfactant, suspension concentration, pH and conductivity [1,4]. EPD is advantageous because it offers the possibility of coating substrates of complex shape, allows accurate control of coating thickness and requires simple equipment [1,5,6]. A distinct group of bioceramics are bioactive glasses (BGs). These are amorphous silicate-based materials, which are classified as osteo-productive, i.e. they can bond to bone and induce new bone growth while dissolving over time when in contact with biological fluids. Bioglass® 45S5 (composition: 45 SiO_2, 24.5 Na_2O, 24.5 CaO, 6 P_2O_5 in wt%) was the first bioactive glass formulation, which was shown to have the ability to bond to the host tissue [7]. The formation of hydroxyapatite (HA) on bioactive glass surfaces upon contact with physiological fluids is responsible for the bone-bonding properties of bioactive glasses [8,9]. These materials stimulate cell attachment [10], and their dissolution products have been shown to control the gene expression in human osteoblastic cells [11,12]. Bioactive

* Corresponding author.
E-mail addresses: namir.jackoub@fau.de (N.S. Radda'a), wgoldmann@biomed.uni-erlangen.de (W.H. Goldmann), rainer.detsch@fau.de (R. Detsch), judith.roether@fau.de (J.A. Roether), lcordero@tec.ac.cr (L. Cordero-Arias), virtanen@ww.uni-erlangen.de (S. Virtanen), tmoskale@agh.edu.pl (T. Moskalewicz), aldo.boccaccini@ww.uni-erlangen.de (A.R. Boccaccini).

http://dx.doi.org/10.1016/j.surfcoat.2017.07.048
0257-8972/

glasses can be combined with a biopolymer to coat metallic implants, forming organic-inorganic composite coatings for the modification of implants in load-bearing areas [3,13]. Chitosan is an interesting polymer that has been widely used to produce a variety of coatings in combination with electrophoretic deposition (EPD) [1,2,13–15]. Due to its biodegradable behavior [16,17], chitosan has been investigated in different forms in orthopedics, for example, to functionalize metallic implants [6,18], as a bone cement additive and as composite biodegradable scaffolds for drug and cell delivery systems [18]. Halloysite nanotubes (HNTs) are novel natural nanomaterials with predominantly hollow tubular nanostructures. HNTs are a type of aluminosilicate clay of the formula $Al_2Si_2O_5(OH)_4 \cdot nH_2O$, where 'n' equals to 0 or 2, representing HNTs, which are dehydrated and hydrated, respectively [19–22]. HNTs have different morphologies but the tubular structure is the most common [19,22,23] with typical dimensions of 1–30 nm in inner diameter and 30–50 nm in outer diameter with 100–2000 μm in length [19,22,24]. HNTs have high mechanical strength and modulus, which makes them ideal materials for preparing different polymer-based composites [19,25,26]. It has been reported [27–33] that HNTs are biocompatible and potentially used as drug delivery vehicles, therefore HNTs-polymer nanocomposites are promising drug releasing carriers [27,34,35]. Nanocomposite coatings containing a polyelectrolyte and halloysite nanotubes can be fabricated using electrophoretic deposition [27,36,37].

The formation of bacterial biofilms on orthopedic implants is a serious medical problem as such biofilms are extremely resistant to both the immune system and antibiotics [38]. For treatment of such conditions, local delivery of drugs can be effective to achieve the desired results [39]. Coating of the implant with a drug releasing and bioactive coating is one of the promising techniques that has been explored for tackling implant infections [40]. Tetracycline hydrochloride (TCN), a polyketide antibiotic, was used as a model drug in this study to show the feasibility of EPD for obtaining drug loaded composite coatings.

Therefore, we suggest the fabrication of TCN-loaded halloysite nanotubes in chitosan/Bioglass® 45S5 composite coatings using EPD. The aim of this research is to explore the antibacterial functionality of TCN-loaded HNTs incorporated in an organic-inorganic composite coating. The novel coatings differ from similar electrophoretic coatings developed previously (e.g. [1,2]) in the enhanced multifunctionality provided by TCN-loaded halloysite nanotubes. Furthermore, to show the EPD potency for obtaining such chitosan/BG/HNTs/TCN composite coatings, SEM/EDX, XRD and FTIR analyses were performed to characterize the coatings. The release of antibacterial agents in phosphate buffered saline (PBS) was investigated by UV spectrometry. Simulated body fluid (SBF) bioactivity tests were performed to assess the potential suitability of the coatings as bone contacting materials. The ability of coatings in preventing bacterial growth was tested using *E. coli* as gram-negative and *S. aureus* as gram-positive bacteria. The attachment, proliferation and cytotoxicity of MG-63 osteoblast-like cells on the fabricated coatings were explored. The adhesion between coatings and substrates was tested by the tape test and surface roughness, contact angle and corrosion behavior tests were performed on fabricated coatings to assess their suitability for possible orthopedic applications.

2. Experimental procedure

2.1. Materials

Chitosan powder (C) with a deacetylation degree of about 85% (MW = 190 kDa), halloysite nanotubes (HNTs) with a tube diameter of 20–90 nm (Fig. 1) and lengths of 70 μm and acetic acid were purchased from Sigma Aldrich (Germany). HNTs were investigated by transmission electron microscopy (TEM) using a JEOL JEM-2010 ARP microscope (Japan) operating at 200 kV. A thin foil for TEM investigation was prepared by dispersing the powder in ethanol and stirring in order to separate agglomerated particles. Finally, a droplet of the stable suspension was placed on a copper grid covered with carbon film and dried. Bioactive glass powder (45S5 BG) used in this study had a median particle size of 2.0 μm (Schott AG. Germany). Tetracycline hydrochloride (TCN) was purchased from AppliChem GmbH-Darmstadt (Germany). Ethanol was purchased from Merck KGaA (Germany).

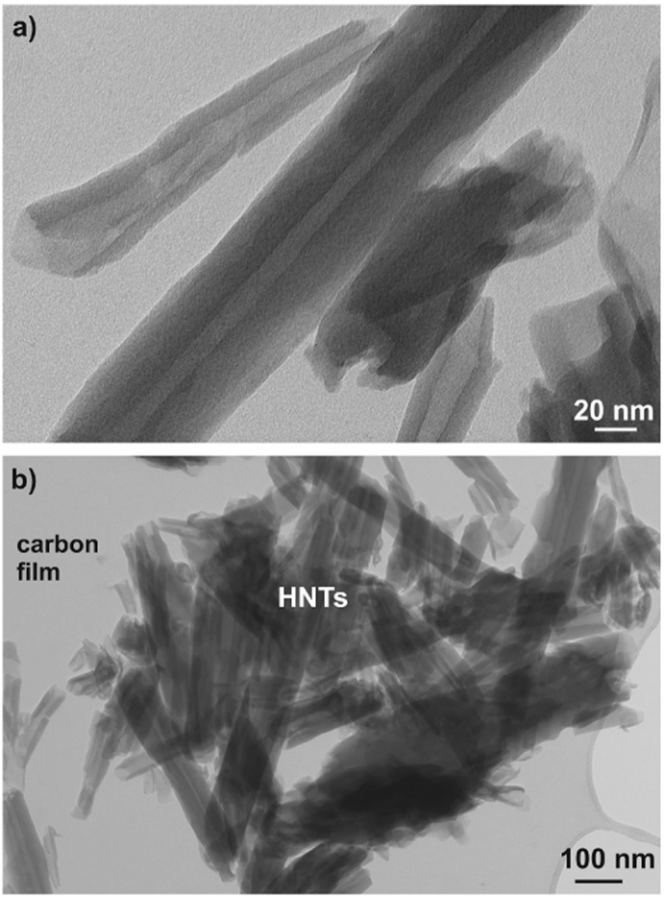

Fig. 1. TEM bright field (BF) micrographs of separate HNTs (a) and HNTs agglomerate (b).

2.2. Loading of HNTs with TCN

The preparation of HNTs loaded with TCN was carried out following a protocol available in the literature [41]: first, TCN (10 mg/L) was dissolved in phosphate buffered saline PBS at 80 °C for 20 min. HNTs (10 mg/L) were then mixed with the drug solution (TCN). The mixture was placed in an ultrasonic bath for 60 min. Vacuum (0.85 bar) was applied for 12 min using a vacuum pump (BRAND GmbH, Germany). The solution was then taken from the vacuum and shaken by hand for 5 min. The application of vacuum was then repeated for 12 min. TCN-loaded HNTs were dried in an oven (Nabertherm, Germany) for 16 h at 50 °C. The dried powders were ground gently using a mortar and pestle. It should be pointed out that in this study the absolute drug loading was not optimized (or considered as a variable) as for each potential application of the coatings a different drug loading may be required. The objective of the experiment was rather to demonstrate the ability to load and release a certain concentration of TCN from the loaded HNTs present in the electrophoretically deposited chitosan based coatings.

2.3. EPD of composite coatings

Chitosan-BG-Halloysite nanotubes with tetracycline (C-BG-HNTs-TCN) composite films were prepared from suspensions containing 2.0 g/L 45S5 BG with 0.5 g/L of chitosan in the blend of HNTs-TCN as

stated above. The chitosan solution was prepared by dissolving chitosan powder in 1 vol% aqueous acetic acid solution. A suspension was prepared by adding the 3.82 g/L of HNTs-TCN blend to the chitosan solution. A mixture of water and ethanol with 75 vol% of distilled water was used. Chitosan-BG-Halloysite nanotubes (C-BG-HNTs) and chitosan-BG (C-BG) composite coatings were prepared with the same amounts and concentrations of materials and solvent as stated above. A constant electric voltage was applied by a Telemeter (Electronic GmbH TTi Ex 752 M 75 V/150 V 300 W) power supply, and the current through the suspension during EPD was monitored by a 1906 Computing Multimeter from Thurlby-Thandar instruments LTD (Huntingdon, England). The current density during the EPD process was monitored to confirm that it was reducing as function of time, which would prove the successful EPD. After a sequence of trial-and-error experiments (data not reported here), which is a common but not satisfactory approach in EPD [1,2], the suitable voltage and deposition time were determined, namely 40 V and 30 s, respectively. The distance between the electrodes (both electrodes were AISI 316L stainless steel foils of dimensions: 30 mm × 15 mm × 0.2 mm) was kept constant at 10 mm. In order to ensure the homogeneity of the coating, the stability of the C-BG-HNTs-TCN suspension was studied in terms of zeta potential, measured by laser Doppler velocimetry (LDV) technique.

2.4. Characterization and coating layer testing

The C-BG-HNTs-TCN composite coatings were characterized using SEM (Smart SEM V05.6 ZEISS, Carl Zeiss Microscopy GmbH, Jena, Germany) with 10 kV accelerating voltage. SEM was used to study surface microstructures and the cross-sections of the deposited coatings. EDX (Oxford Instruments SSD-detector) was used for qualitative, elemental analysis of the coatings at 20–30 kV SEM operating voltage. The crystalline phases present in the EPD coatings were identified by X-ray diffraction (XRD) analysis. The diffractograms were obtained using an X-ray diffractometer (D500 Siemens, Siemens, München, Germany) and a CuKα 1.2 secondary-Monochromator with 0.02° as a 2θ step in the range of 5° to 70° operated at 30 kV. Fourier transform infrared (FTIR) spectroscopy (Nicolet 6700, Thermo Scientific, Waltham, MA, USA) measurements were performed to record spectra of the coated samples in the wave number range of 400–4000 cm^{-1}. The adhesion between coatings and substrates was tested by the tape test (cross-cut-adhesion test) according to the ASTM D3359 method B [42] using an Elcometer 107 cross-hatch-cutter (Manchester, UK). The surface roughness values were measured by a laser profilometer (UBM, ISC-2). The values include (Ra) as the average roughness, (Rz) as the mean peak to valley height, and (Ry) as the maximum peak to valley height. Static water contact angle measurements with a DSA30 instrument (Kruess GmbH, Germany) were applied to evaluate the wettability of deposited coatings. An electrochemical evaluation in cell culture medium was performed to investigate the corrosion behavior of coated and uncoated substrates. Polarization curves were obtained using a potentiostat/galvanostat device (Autolab PGSTAT 30, Deutsche Metrohm GmbH, Filderstadt, Germany). The samples were immersed in 100 mL of Dulbecco's MEM (DMEM, Biochrom) at 37 °C. A conventional three electrode system was used, where a platinum foil served as counter electrode and Ag/AgCl (3 $mol \cdot dm^{-3}$ KCl) was used as reference electrode. The analysis was carried out using an O-ring cell with an exposed sample area of 0.38 cm^2 with a potential sweep rate of 1 mV/s.

2.5. In vitro bioactivity tests

In-vitro bioactivity assessments were carried out in simulated body fluid (SBF) prepared according to Kokubo et al. [43]. The C-BG-HNTs-TCN coated samples were immersed in 50 mL of SBF and incubated at 37 °C for 3 and 7 days. After immersion in SBF, the substrates were dried at room temperature. FTIR and XRD analyses were performed on the SBF treated samples to analyze possible hydroxyapatite (HA) formation on the surface, which is an indicator of the bioactivity in the context of bone contacting materials [43].

2.6. In vitro cellular studies

2.6.1. Preparation

C-BG and C-BG-HNTs coated samples were sterilized in a furnace (L3/11 B180, Nabertherm-Germany) at 160 °C for 3 h [44], and the C-BG-HNTs-TCN coated samples were sterilized in a UV chamber (Whatman Biometra T1, Germany) for 60 min. The coated samples were 12 mm in diameter (316L SS). The samples were incubated in Dulbecco Modified Eagle Medium (DMEM) (Gibco) with 10 vol% fetal calf serum and 1 vol% of penicillin-streptomycin) for 48 and 72 h, respectively, in an incubator (ThermoScientific) at 37 °C with 5 vol% CO_2 and 95% humidity. In parallel, MG-63 cells (obtained from ATCC) were harvested from the cell culture flask and placed in a 96-well plate. Subsequently, 10^4cells in 1 mL of cell culture medium were pipetted on each sample.

After 48 and 72 h of incubation time, respectively, cell viability and cell proliferation tests were performed. The preparation was done according to the biological evaluation of medical devices, part 5 tests for in vitro cytotoxicity, of ISO 10993-5. The results were reported as mean ± standard deviation. One-way analysis of variance (ANOVA) with $p < 0.05$ as significance level was utilized for statistical analysis. Fluorescence microscopy was used to assess the cell viability. SEM images were performed to characterize the cell morphology.

2.6.2. Cell viability studies

Viability studies were carried out using WST (Water-soluble tetrazolium salt) measurements following standard protocols (Sigma-Aldrich cell counting kit 8). In short, the cell culture medium was removed from the cells. C-BG, C-BG-HNTs, and C-BG-HNTs-TCN coated samples were washed with PBS. PBS was then removed, and a mastermix (containing 1%WST reagent in cell culture medium) was added to the coated samples. After 2 h of incubation, 100 μL of the supernatant of each sample was put in a 96-well plate, and the absorbance of the liquid was measured by a plate reader (Anthos-Phomo, Germany) at 450 nm.

2.6.3. Cell proliferation studies

The proliferation of cells was determined using BrdU (Bromodeoxyuridine) measurements (colorimetric) according to Roche-version 14.0-Cat. No. 11 647 229 001.

2.6.4. Fluorescence microscopy tests

Cell viability was determined by Calcein-AM and DAPI staining. Cells were washed with PBS. A mastermix containing 5 μg Calcein-AM per mL PBS was added to the cells. After incubation for 45 min, samples were washed with PBS and fixed with a 3.7 wt% paraformaldehyde (PFA Sigma-Aldrich, Germany) containing solution for 15 min. Cells were washed with PBS, and a mastermix containing 1 μg DAPI per mL PBS was added to the samples for 5 min. The cells were left in PBS until microscopic analysis. A fluorescence microscope (AXIO Scope A1, Zeiss) was used to observe the residual cells.

2.7. Tetracycline hydrochloride release studies

In vitro release kinetics of tetracycline hydrochloride was measured using a UV spectrometer (Analytik, Jena SPECORD 40, Germany) at a wavelength of 362 nm. Coated samples were studied by incubating them (substrate with coated area of 1.76 cm^2) in 4 mL PBS from Sigma (pH = 7.3 ± 0.2 at 25 °C) at 37 °C. Aliquots of 4 mL (the total release volume) were withdrawn from samples at predetermined times of 3, 5, 7, 14, 21, 28, 35 and 42 days, and replenished by fresh PBS. 1 mL of PBS from each sample was collected at regular intervals for

measurement. Three samples of each predetermined times were prepared, and the readings were averaged for each time point.

2.8. Antibacterial studies

The investigation of the antibacterial properties of C-BG, C-BG-HNTs, and C-BG-HNTs-TCN composite coatings was carried out using gram-negative (*E. coli*) and gram-positive bacteria (*S. aureus*), respectively. LB (lysogeny broth) agar was used to completely cover the surface of the Petri dishes (about 20 mL). The bacteria were taken from a colony of bacteria and mixed with 5 mL of LB Medium (Carl Roth GmbH, Karlsruhe, Germany). The bacterial cells were placed in the incubator overnight at 37 °C, and the solution was then diluted to an optical density OD_{600nm} of ~0.015 (Eppendorf, Biophotometer, Hamburg, Germany). 20 μL of the bacteria solution and 40 μL from LB medium were placed on each sample by a pipette. The samples with bacteria drops were incubated to permit the bacteria to grow for 2, 4, 12, and 24 h, respectively. After each time period, one sample was stamped on an agar plate, and the plates were then incubated to let the bacteria grow for 24 h. Afterwards, to quantitatively assess the growth of the bacteria cells, photographic images were taken.

3. Results and discussion

3.1. Drug loading in HNTs

The outer surface of HNTs is the result of Si—O—Si negatively charged bonds, while the inner surface is from Al(OH) positively charged bonds [41,45]. The electrostatic attraction between the cationic drug (TCN) and the negatively charged outer surface of HNTs leads to the adsorption of TCN onto the surface. The positively charged lumen of the HNTs (inner surface) could attract TCN molecules during the vacuum process [41,46,47]. The negative pressure effect possibly creates the driving force to encapsulate TCN within the lumen of HNTs, independently of the similarity of charge polarity of TCN and HNTs. The loading of TCN was carried out in BPS buffer at pH 7.4 to prevent neutralization of TCN with positive charges, which is not useful for the electrostatic interaction with the HNTs.

3.2. EPD process of C-BG-HNTs-TCN composite coatings

Composite films were prepared from a suspension of BG and TCN-loaded HNTs in chitosan solutions. The presence of chitosan in the system can provide the necessary positive charge to perform EPD, as

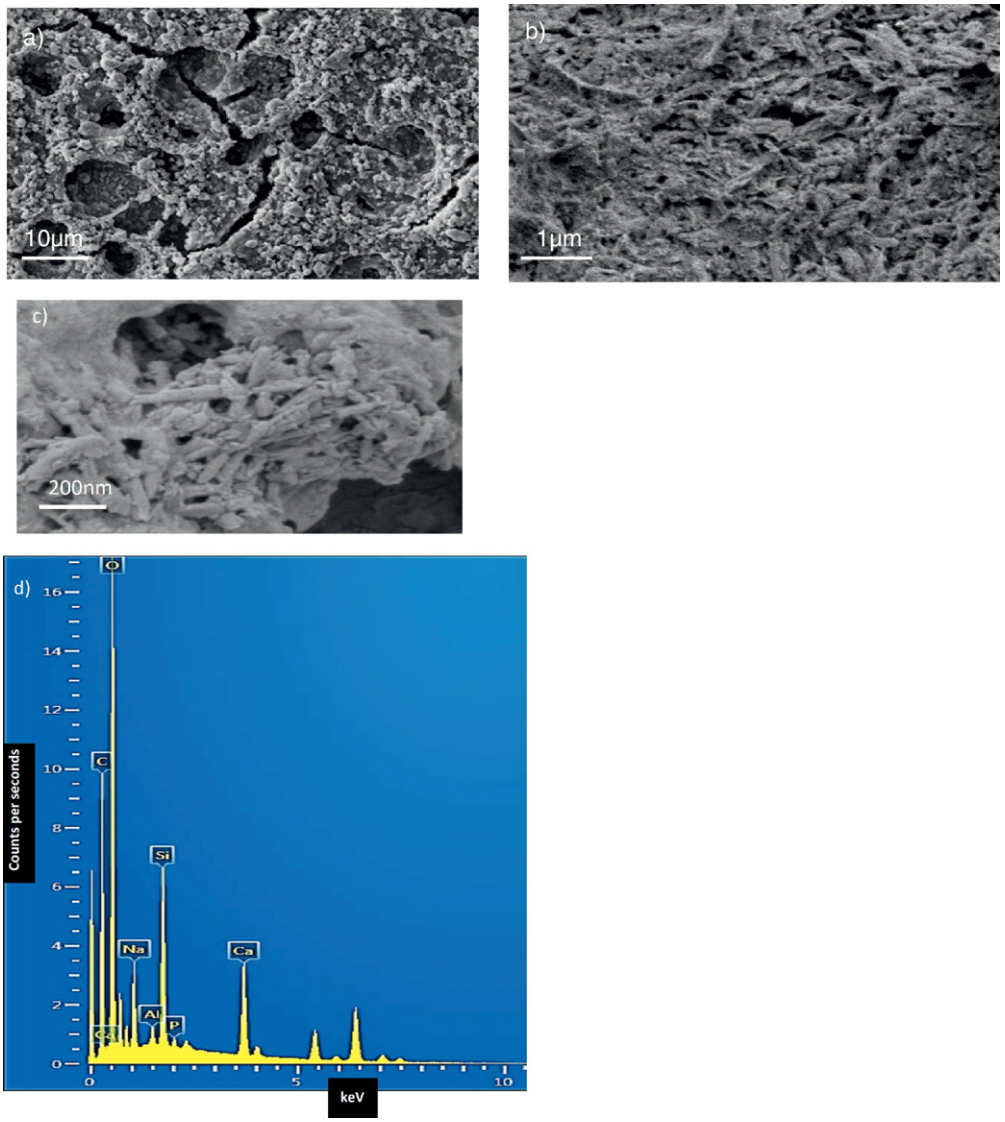

Fig. 2. SEM images of C-BG-HNTs-TCN coating at (a) lower, (b, c) higher magnifications and (d) EDX spectrum corresponding with panel a.

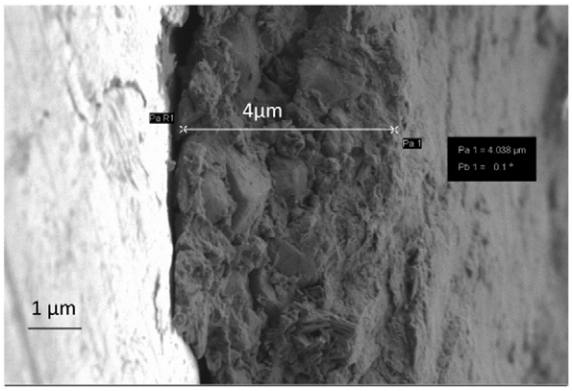

Fig. 3. SEM image showing the cross-section of a C-BG-HNTs-TCN composite coating.

discussed extensively in the literature [48–50], and it contributes to the suspension stabilization. Based on similar observations on chitosan-inorganic particle systems [50,51], a deposition mechanism can be suggested that involves the adsorption of positively charged chitosan molecules on negatively charged BG micron-sized particles [51] and on TCN loaded HNTs. In addition, non-adsorbed chitosan molecules and HNTs present in the bulk of the suspension can be also incorporated in the deposited layer by direct EPD. The zeta potential of C-BG-HNTs-TCN suspensions was $+79 \pm 4$ mV at the working pH of 4.0, which predicts cathodic deposition of the particles. Therefore, the simultaneous deposition of chitosan, 45S5 BG particles and HNTs-TCN can be combined to form a composite film on the cathode.

3.3. Composition and microstructure of C-BG-HNTs-TCN composite coatings

The morphology and cross-section of selected coatings were characterized by SEM. The microstructure of the C-BG-HNTs-TCN coating at both low and high magnification is shown in Fig. 2a and b, respectively. It is apparent that the coating consists of a chitosan matrix containing BG particles and halloysite nanotubes. Fig. 2a shows the presence of microcracks in the coating structure probably formed by differential shrinkage upon drying of the composite layers. While such microcrack formation should be minimized, for example by reducing coating thickness, it was apparent that the adhesion strength between coating and substrate was satisfactory in the present study (see results in Section 3.5), which indicates that the formation of cracks did not result in reduced structural integrity of the coatings, probably due to the ability of chitosan to penetrate the interspaces between BG particles and HNTs, acting as a continuous matrix adhered to the substrate. In Fig. 2c halloysite nanotubes can be observed in the C-BG-HNTs-TCN coating. The EDX spectrum in Fig. 2d contains peaks associated with Ca, Si, P, and Na atoms, which are the constituents of 45S5 BG. The peaks of Al indicate the presence of halloysite, which contains mainly Si and Al. Finally, the 'C' peak in Fig. 2d can be related to chitosan and tetracycline. An SEM image of the cross-section of C-BG-HNTs-TCN coating (Fig. 3) shows that the film is fairly uniform at a microscale. The thickness was around 4 µm.

The composition and structure of the deposited coatings were investigated by FTIR (before and after immersion in SBF). FTIR analysis of the C-BG-HNTs-TCN coating is shown in Fig. 4. The peaks corresponding to the stretching vibration O—H at 3463 cm^{-1} [51], carbonyl bond C—O in the amide group at 1640 cm^{-1} [51], and N—H bending vibration of the amine group at 1568 cm^{-1} [51,52] are observed. Si—O—Si bending vibration appears at 470 cm^{-1}, and Al—O—Si deformation in HNTs can be detected at 538 cm^{-1} [53,54]. The peak at 790 cm^{-1} is assigned to Si—O stretching [53,54]. N—H stretching in amine and amide at 3371 cm^{-1} are shown as well as the stretching vibration peaks at 920 cm^{-1} and 1030 cm^{-1}, which are indicative of Na and Ca [51,55]. All these peaks indicate that chitosan, BG, HNTs, and TCN are incorporated in the coating. After immersion in SBF for three and seven days, respectively, a reduction in the heights of the peaks related to BG (Si—O—Si at 470 cm^{-1}) and the formation of new bonds such at 564 cm^{-1}, 605 cm^{-1}, 960 cm^{-1}, and 1037 cm^{-1}, respectively, are observed, which were assigned to phosphate formation [51]. The peaks at 873 cm^{-1} and 1421 cm^{-1} are assigned to carbonate formation [51]. Phosphate and carbonate formation indicate the presence of hydroxyl carbonate apatite (HCA).

The XRD patterns of C-BG-HNTs-TCN coatings (before and after immersion in SBF) are shown in Fig. 5. As shown, the diffraction peaks corresponding to HNTs appear in the coatings, while peaks corresponding to TCN are also present. The crystalline structure of the new phase exhibits XRD peaks at 32° and 46° matching those of the standard pattern of hydroxyapatite (HA) crystals. All peaks were indexed, using the JCPDS file of 01-001-1008, 00-013-0375, and 00-013-0742 for HA, HNTs, and TCN, respectively.

3.4. Corrosion behavior

The possible corrosion protection effect of the C-BG-HNTs-TCN composite coatings was investigated. The intention was to assess if such complex drug loaded coatings could provide protection based on the fact that similar chitosan-inorganic particle coatings have already

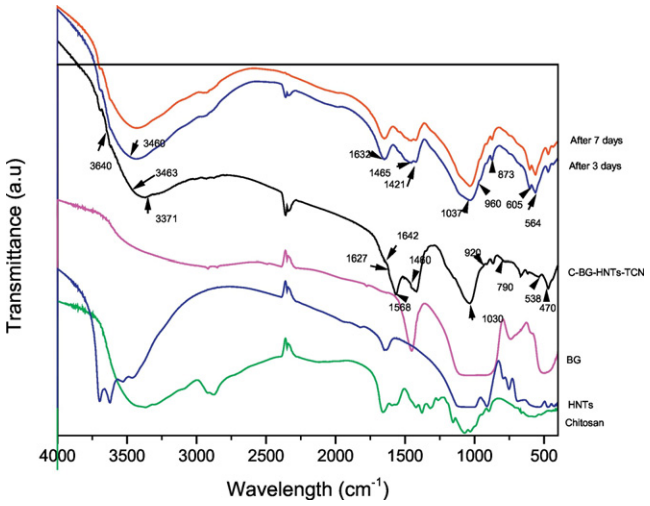

Fig. 4. FTIR spectra of chitosan powder, HNTs powder, BG powder, and C-BG-HNTs-TCN coating before and after the immersion in SBF for 3 and 7 days, respectively.

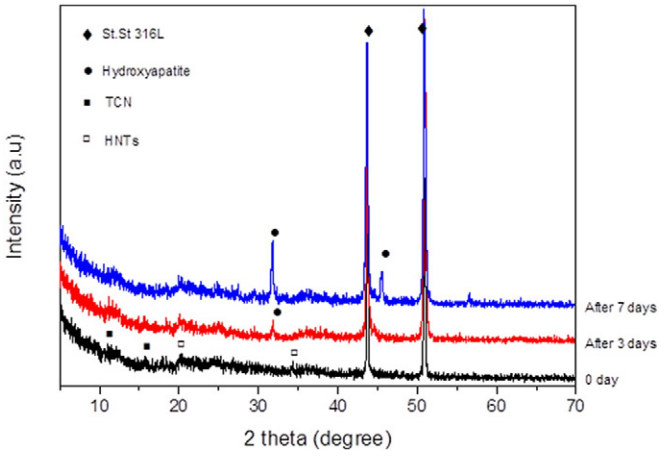

Fig. 5. XRD patterns of C-BG-HNTs-TCN coating before and after immersion in SBF for 3 and 7 days.

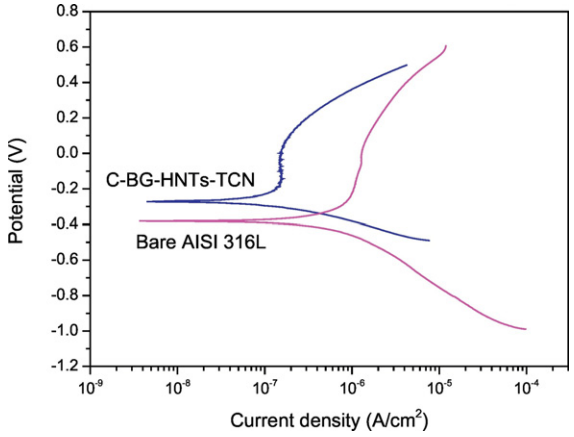

Fig. 6. Polarization curves in DMEM for bare SS 316L substrate and for SS coated with a film of C-BG-HNTs-TCN suspension at 37 °C.

shown protective effects [1,2]. Fig. 6 shows the polarization curves for the C-BG-HNTs-TCN coating and the bare stainless steel substrate. It can be observed that the coated system shows a higher E_{corr} (corrosion potential) and a lower i_{corr} (corrosion current density) compared to the uncoated metallic substrate, indicating that the composite coating protects the substrate against corrosion. Slowing down the kinetics of both anodic and cathodic reactions may be viewed as an indication of the corrosion protective properties of this coating. Even if gaps caused by BG dissolution are likely to leave a space to enable DMEM to penetrate into the coating and to create micro-defects [56], the reduction of the current density can be ascribed due to the presence of small particles of HNTs, which are able to fill the gaps among agglomeration of the larger particles, leading to a decrease of the substrate surface directly exposed to the corrosion medium. This effect has been previously reported for other BG containing composite coatings [56].

3.5. Adhesion tests

The adhesion strength between C-BG-HNTs-TCN coating and the SS 316L substrate was assessed by the adhesive tape test. The result of the adhesion strength for the coating according to the ASTM D3359-B standard [42] showed that the adhesion strength corresponds to class 4B (Fig. 7). Deen et al. (2012) found that the adhesion strength

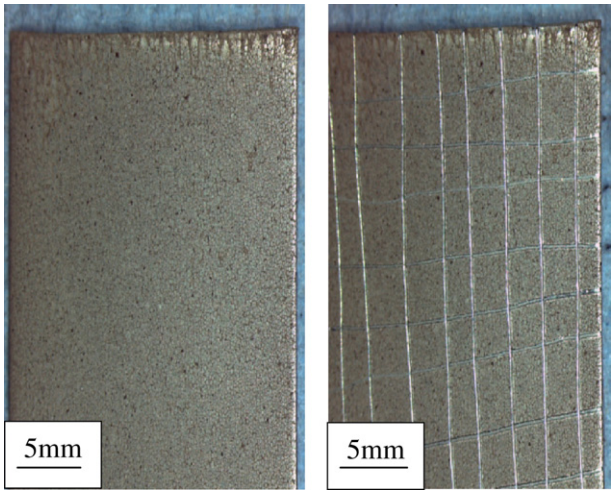

Fig. 7. Typical light microscopy images of coatings before (left) and after (right) adhesive tape tests for C-BG-HNTs-TCN (prepared from suspension containing 2.0 g/L 45S5BG with 0.5 g/L of chitosan and the blend of HNTs-TCN at 40 V and deposition time of 30 s).

Table 1
Surface roughness parameters of deposited coatings.

Sample code	Roughness/μm		
	Ra	Rz	Ry
C-BG-HNTs-TCN	2.10 ± 0.05	11.5 ± 0.3	16.0 ± 1.0
C-BG-HNTs	1.76 ± 0.04	9.4 ± 0.3	12.5 ± 0.9
C-BG	0.50 ± 0.09	5.3 ± 0.4	7.3 ± 0.3

for C-HNTs coatings on 304 SS substrate is class 2B [36], whereas Molaei et al. (2016) observed that C-HNTs coatings on titanium substrate exhibited an adhesion class of 2B [57]. On the other hand, a relatively strong adhesion of C-BG coatings on 316L SS substrate was confirmed [58]. The homogeneous dispersion of HNTs and microsized particles of BG in the matrix gives a relatively high surface area, allowing chitosan to penetrate the interspaces between BG particles and HNTs, which results in an overall improved attachment between the coating layer and the substrate.

3.6. Wettability behavior

The wettability of the composite films, namely C-BG-HNTs-TCN, C-BG-HNTs and C-BG, was evaluated using static water contact angle measurements. The average measured values were 50.2 ± 0.9°, 56 ± 1.0° and 69 ± 1.0° for C-BG-HNTs-TCN, C-BG-HNTs, and C-BG coatings, respectively. These values are within the range of 35° to 80°, which has been suggested in literature [59,60] as being relevant for orthopedic applications because they should lead to good solid-liquid interaction inducing suitable cell spreading [61]. The above results also indicate high surface energies for all coatings [62]. The reason for the decrease of contact angle in C-BG-HNTs-TCN compared to C-BG composite coatings could be due to the higher surface roughness of the coatings, as shown in the next section. Li et al. (2015) reached this conclusion when they prepared C, C-BG, and C-BG- PHBV membranes, in which the rougher surface (C-BG-PHBV) exhibited the lowest contact angle [63].

3.7. Roughness measurements

The values of Ra, Rz and Ry for C-BG-HNTs-TCN, C-BG-HNTs, and C-BG coatings are shown in Table 1.

According to the above results, the average roughness values are generally higher for coatings especially for C-BG-HNTs-TCN and C-BG-HNTs, respectively. This behavior is probably due to the greater amount

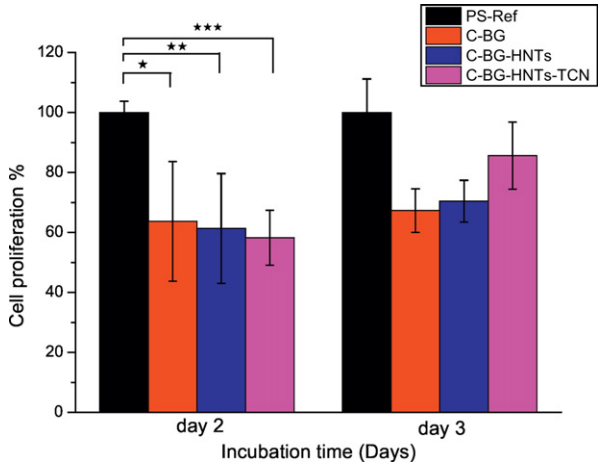

Fig. 8. Proliferation percentage rate of MG63 cells cultured on C-BG, C-BG-HNTs, and C-BG-HNTs-TCN coatings measured by BrdU test after 2 and 3 days, respectively. Tissue culture plastic (polystyrene, PS) was used as control at the same time period. According to the ANOVA test * is significant for PS vs. C-BG, ** for PS vs. C-BG-HNTs, and *** for PS vs. C-BG-HNTs-TCN on day 2.

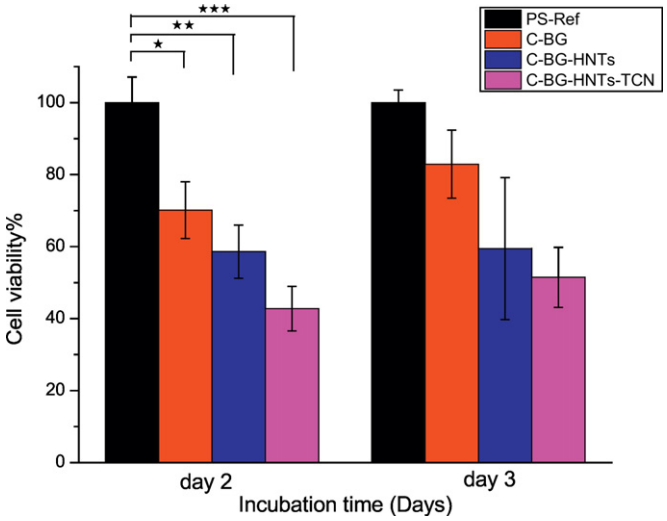

Fig. 9. Cell viability of MG63 cells cultured on C-BG, C-BG-HNTs and C-BG-HNTs-TCN coatings measured by WST1 test after 2 and 3 days of culture. Tissue culture plastic (polystyrene) (PS) was used as the control. According to the ANOVA test * is significant for PS vs. C-BG, ** for PS vs. C-BG-HNTs, and *** for PS vs. C-BG-HNTs-TCN on day 2.

of filler material in this type of coating. There is a correlation between increased implant surface roughness and improved cell adhesion and proliferation [64,65]. Cells can probably attach more strongly to surfaces with a rougher topography than to smooth surfaces, and they can orient themselves in the grooves, as demonstrated by Chehroudi et al. [66,67] and Brunette [68]. It has also been reported that osteoblast cells attach better to rough titanium surfaces than to smother surface polished with diamond paste [69].

3.8. In vitro cytocompatibility tests

The cellular activity of MG63 cells cultured on fabricated samples was measured by the cell proliferation (Brdu test) and cell viability tests (WST1 test). MG63 cells were cultured on C-BG, C-BG-HNTs and C-BG-HNTs-TCN coatings, respectively. Polystyrene (PS) was used as control. The results are shown in Fig. 8, which indicate that there is no significant difference ($p < 0.05$) between the C-BG-HNTs-TCN coating and the control (100%) after 3 days. On the other hand, there is a statistically significant difference ($p < 0.05$) for all three investigated coatings when compared with the polystyrene control after 2 days in culture. After 3 days in culture, an increase in cell viability as assessed by BrdU can be observed for all 3 coatings. The fact that there is no statistically significant difference between the C-BG-HNTs-TCN coating and the PS

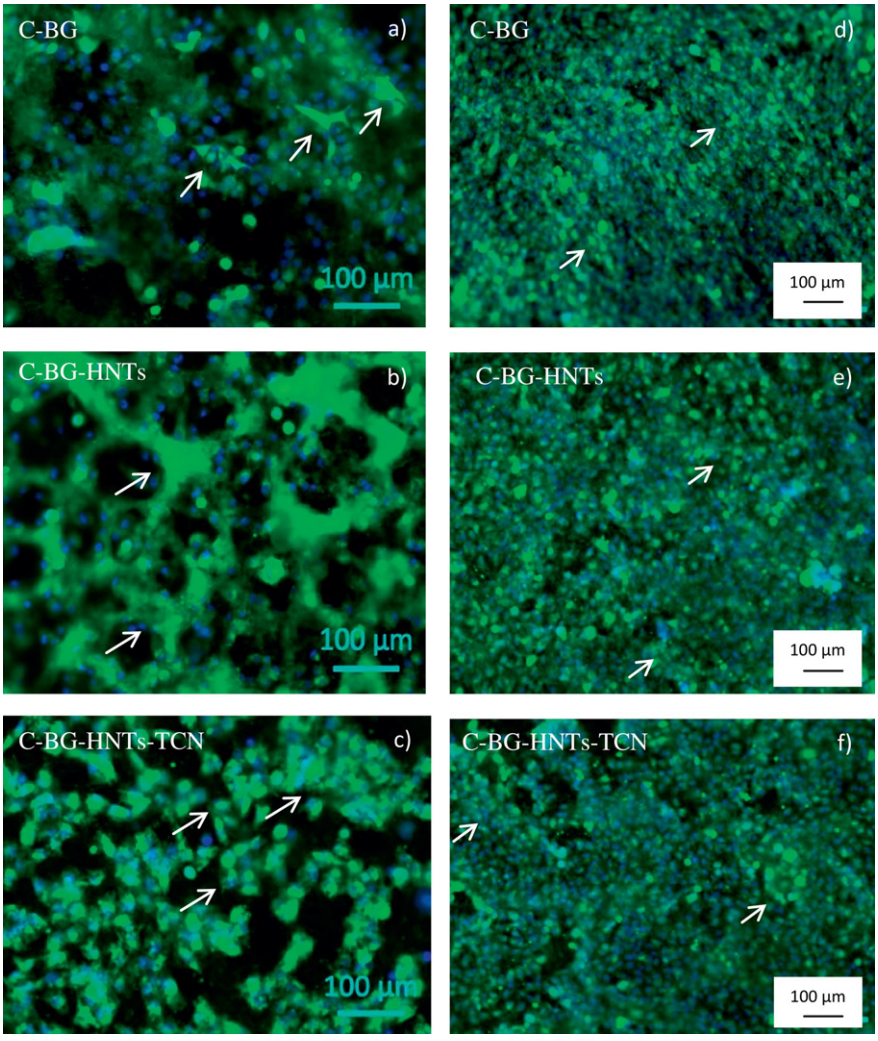

Fig. 10. Fluorescence images of MG63 cells cultured on C-BG, C-BG-HNTs and C-BG-HNTs-TCN coated on SS for 2 days (a, b, c) and 3 days (d, e, f), respectively. Live cell staining in green (Calcein-AM) and nuclei in blue. The marked areas (white arrows) are areas of increased cell growth.

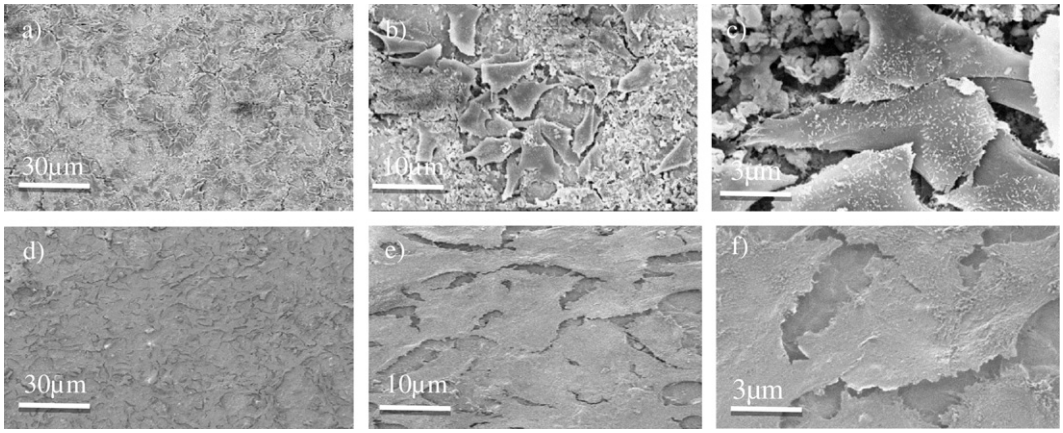

Fig. 11. SEM images of C-BG coating after seeding with MG63 cells for two days (a, b, c) and three days (d, e, f), respectively, at different magnifications.

control after 3 days indicates that the cell proliferation on the coated samples and the control was similar.

The WST1 test is a measure of cell viability (Fig. 9), which demonstrates that on day 2 the cell viability was ~42% (±6) for C-BG-HNTs-TCN, ~58% (±7) for C-BG-HNTs, and ~70% (±8) for C-BG coatings. The reason for reduced cell viability compared to the PS control might be the release of TCN and HNTs and inorganic compounds from BG, negatively affecting the MG63 cell viability. On day 3, the cell viability for C-BG-HNTs did not change significantly (from 58% to 59%). This result could be due to the high concentration of HNTs. However, an increase in cell viability could be observed for C-BG and C-BG-HNTs-TCN coatings to around 83% (±9) and 51% (±8), respectively. For C-BG, the increase in cell viability from day 2 to day 3 is significant. On day 3, the difference in cell viability between the PS control and the C-BG coating is no longer significant. For C-BG-HNTs-TCN composite coatings, it must be determined whether the amount of TCN in the coating needs to be reduced. In the present experiments, three important factors can affect the cell viability, namely: porosity, surface chemistry and surface roughness [70–74]. The composite coatings, C-BG, C-BG-HNTs and C-BG-HNTs-TCN depicted surface roughness (Ra) (reported in the previous Section 3.7) over 0.5 µm, which could explain the preference of osteoblasts to these surfaces [75]. On the other hand, the wettability of the surface, measured in terms of water contact angle (reported in the previous Section 3.6), reflects appropriate results for bone regenerative applications [76,77]. In addition, the increasing cell viability for C-BG-HNTs-TCN composite coatings from 2 to 3 days confirms that tetracycline has not increased the cytotoxicity level of the composite coatings. According to the literature [78], for long-term exposure to tetracycline, an increase in the viability and proliferation of osteoblastic cells can occur. In this study, it is expected that an improvement in the cell viability will occur at longer incubation times.

Fluorescence images of MG-63 cells, shown in Fig. 10, indicate evidence of cells growth in islands on the coatings structure and their viability. Qualitatively, the cell formation indicates suitable adhesion of cells on the investigated surfaces.

3.9. Cell morphology

The morphology of MG63 cells seeded on the surface of C-BG, C-BG-HNTs and C-BG-HNTs-TCN coated samples after two and three days are shown in Figs. 11–13, respectively. After cultivation, the cells adhered on the surface of C-BG as shown in Fig. 10, indicating that BG significantly promotes the adhesion of MG-63 cells. This result demonstrates that BG particles induced an increase of the surface roughness of the composite coatings that might assist the anchoring and attachment of cells to the surface [63,79,80]. The cells show good adhesion and spreading after two and three days of culture for C-BG-HNTs and C-BG-HNTs-TCN composite coatings. This behavior may be attributed to an increase of the surface roughness caused by adding HNTs particles to the coatings (as shown in Table 1, Section 3.7). Under higher magnification, as observed in Fig. 11 c, f, 12 c, f and 13 c, f, respectively, the cells appear to be flat, probably adhering tightly to the coating surfaces, indicating favorable cell material interactions. The first phase of tissue-implant interaction involves cell attachment, adhesion and spreading. The

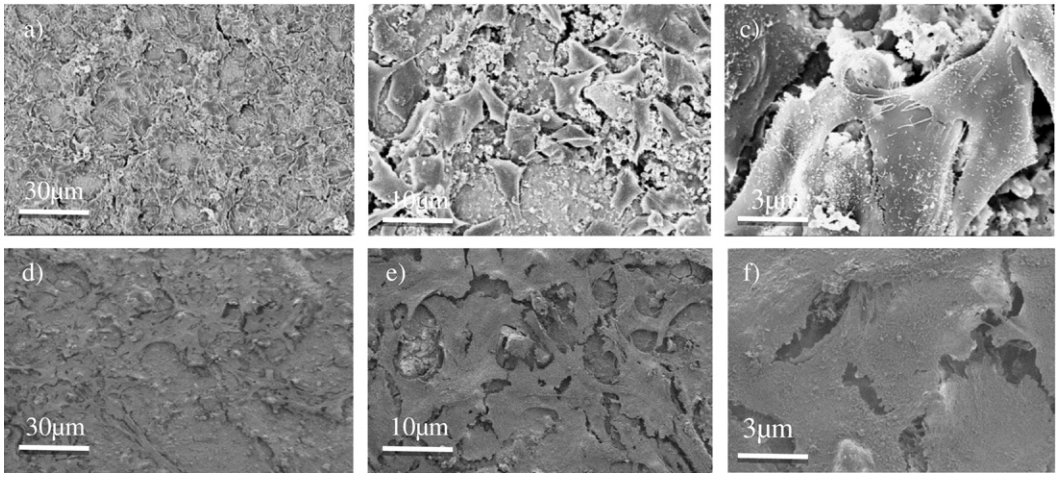

Fig. 12. SEM images of C-BG-HNTs coating after seeding with MG63 cells for two days (a, b, c) and three days (d, e, f), respectively, at different magnifications.

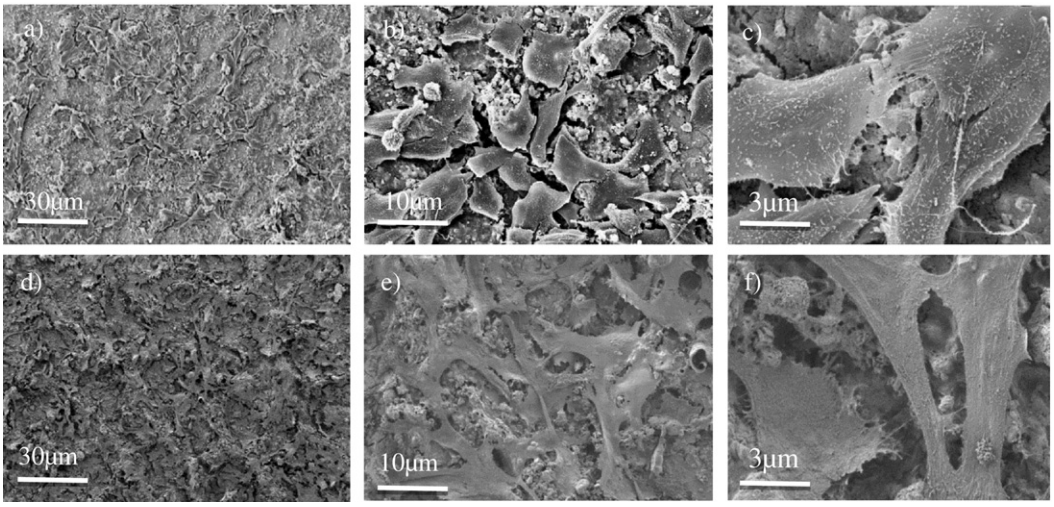

Fig. 13. SEM images of C-BG-HNTs-TCN coating after seeding with MG63 cells for two days (a, b, c) and three days (d, e, f), respectively, at different magnifications.

characteristics of these phases are known to have a large effect on the behavior of cells in terms of proliferation and differentiation [81]. The results confirm that the EPD coatings support attachment and growth of cells over 3 days in culture. Pishbin et al. (2014) observed similar results (good adhesion and spreading of cells), when MG63 cells were seeded on C-BG and C-BG-gentamycin composite coatings and confirmed the growth of cells over 7 days [51].

3.10. Drug release studies

The TCN release profile in PBS from C-BG-HNTs-TCN coatings is shown in Fig. 14. More than 54% of the loaded antibiotic was released within 14 days of immersion in PBS. After the initial burst release, the concentration of the drug in the medium increased more slowly up to 42 days and reached up to 73.2% (116.87 ± 2 μg/cm^2). It can be stated that the release rate of TCN from the composite coating was sustained. The reason for the lower release rate of TCN in the composite coatings compared with previous reported results [46,47] may be attributed to two factors. The first is related to the bonding between TCN and HNTs, in which the TCN release rate was dominated by the equilibrium between dissolution in the medium and the bonding with HNTs. The second is the diameter of the HNTs used in this study (30–70 nm) and the large surface area (64 m^2/g), which should give rise to strong interparticle interactions, leading to a slower release after day 7 [28,41]. In addition to this, Mario et al. [82] suggested that the matrix porosity is a factor on which the drug release kinetics depends on. In our study, the coatings are relatively porous and have a low weight per cent of chitosan, which means that a short time is required for the drug molecules to diffuse, i.e. the drug release can be affected by drug dissolution and diffusion in the liquid, which fills the pores. It has been demonstrated that the dissolution of the drug at the matrix/release medium interface gives rise to a burst release, which is followed by a slower release rate [82]. Xue et al. (2004) added another reason considering that the existence of amino and hydroxyl groups in the tetracycline molecule gives rise to the formation of hydrogen bonds with the hydroxyl moieties of 45S5 Bioglass® [83]. The drug release kinetic is favorable as it should not only facilitate an effective initial antibacterial effect but also it could promote long-term protection against infection.

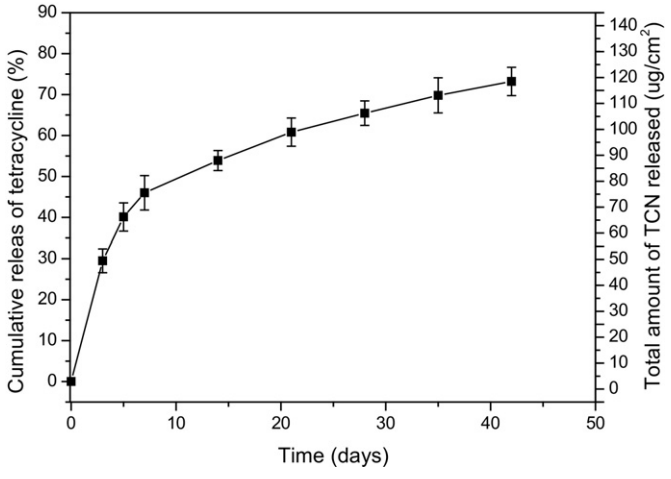

Fig. 14. Cumulative release of tetracycline from C-BG-HNTs-TCN coatings in PBS (the data indicate mean ± standard deviation for three individual experiments).

3.11. Antibacterial tests

Antibacterial tests were carried out with two relevant strains of bacteria (*E. coli and S. aureus*) associated with bone infections. Fig. 15 (a) and (b) show the SS surface as a control for bacteria growth (*E. coli* and *S. aureus*) at various time points. Fig. 15 (c) and (d) indicate the effect of C-BG on bacterial colony formation, especially after 24 h, which can be attributed to the presence of chitosan and BG as previously reported [84,85]. The effect is probably due to an increase in pH of the medium caused by the dissolution of BG. The C-BG coating appears more active against the gram-negative bacteria, *E. coli*. Fig. 15 (e) and (f) showed a stronger antibacterial effect in C-BG-HNTs, which is likely to be the cause of HNTs. Fig. 15 (g) and (h) show an even stronger antibacterial effect for both bacteria types with the composite coating C-BG-HNTs-TCN compared to C-BG-HNTs, where tetracycline shows an effect for both bacteria types. The combination of HNTs and TCN is thus the most effective antibacterial surface coating. Table 2 summarizes the bacterial results described above.

4. Conclusions

C-BG-HNTs coatings incorporating TCN were obtained by cathodic electrophoretic deposition from a stable water/ethanol suspension. Homogeneous and well attached coatings were produced, using a deposition potential of 40 V and over 30 s of deposition. The presence of all components in the coatings was demonstrated using FTIR, XRD, SEM and EDX. HA formation was reported after 3 days of immersion in SBF, confirming the effect of BG in promoting bioactivity. Tetracycline hydrochloride was successfully integrated into the coatings without disruption of the suspension stability, deposition conditions or coating

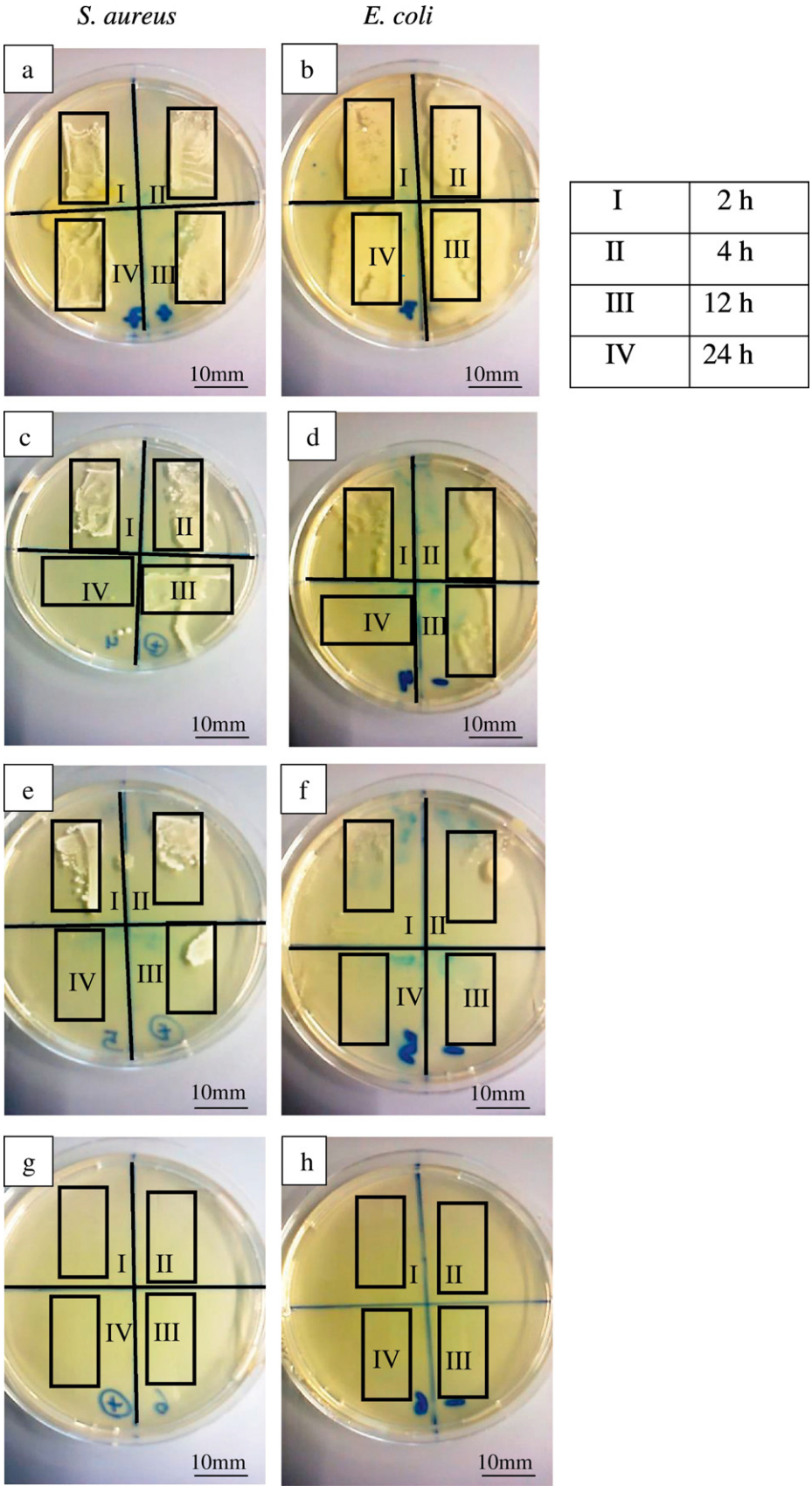

Fig. 15. Antibacterial studies of (a) SS against *S. aureus*, (b) SS against *E. coli*, (c) C-BG against *S. aureus*, (d) C-BG against *E. coli*, (e) C-BG-HNTs against *S. aureus*, (f) C-BG-HNTs against *E. coli*, (g) C-BG-HNTs-TCN against *S. aureus*, and (h) C-BG-HNTs-TCN against *E. coli* for different time periods, i.e. 2 h (I), 4 h (II), 12 h (III) and 24 h (IV).

Table 2
Semi-quantitative analysis for gram-positive and gram-negative bacteria, where ++++ means a lot of bacteria, +++ less of bacteria, ++ little of bacteria, + least of bacteria, and ___ no bacteria left.

Coatings / Time	SS (no coating)		C-BG		C-BG-HNTs		C-BG-HNTs-TCN	
	(a)	(b)	(c)	(d)	(e)	(f)	(g)	(h)
2 h	++++	++++	+++	++	+++	+	___	___
4 h	++++	++++	+++	++	++	+	___	___
12 h	++++	++++	+++	++	+	____	___	___
24 h	++++	++++	___	___	___	____	___	___

homogeneity. For the first time in this study, TCN was successfully loaded into HNTs and deposited as a composite coating by EPD. TCN (54%) was released within 14 days, followed by a prolonged drug delivery period of 42 days to release 73.2% of the initial load. The release kinetics exhibited thus a burst release, and the remaining dose was then released slowly by achieving a therapeutic level. According to the results of cell viability using MG-63 cells, the amount of TCN loaded in the coatings supported cell viability and proliferation of osteoblasts on C-BG and C-BG-HNTs films after 3 days of culture. No significant difference was observed between the films. This implies that the multi-functionalization process of adding tetracycline has not increased the cytotoxicity level of the composite coatings. Cell morphology observation confirmed good adhesion and spreading after two and three days of culture for C-BG-HNTs coatings loaded with TCN. The C-BG-HNTs coating loaded with TCN showed suitable adhesion strength to the substrate. Enhanced corrosion resistance compared to the bare 316L SS substrate was confirmed, showing that C-BG-HNTs-TCN coating provides corrosion protection. Bacterial studies using *E. coli* and *S. aureus* showed the antibacterial effect of all coatings, namely, C-BG, C-BG-HNTs and C-BG-HNTs-TCN, on planar substrates. The antibacterial effect was significantly higher when the coating was loaded with TCN. Summarizing the results, the possibility to produce robust bioactive and antibacterial C-BG-HNTs-TCN coatings using EPD was demonstrated, and the results suggest that the coatings have the potential for orthopedic applications.

Acknowledgements

The government of Iraq is acknowledged for the fellowship to Dr. Namir Radda'a. Experimental support from Ms Alina Grünewald, Institute of Biomaterials, Univ. of Erlangen-Nuremberg, is highly appreciated.

References

[1] N. Raddaha, L. Cordero-Arias, S. Cabanas-Polo, S. Virtanen, J.A. Roether, A.R. Boccaccini, Electrophoretic deposition of chitosan/h-BN and chitosan/h-BN/TiO_2 composite coatings on stainless steel (316L) substrates, Materials 7 (2014) 1814–1829.
[2] L. Cordero-Arias, S. Cabanas-Polo, H.X. Gao, J. Gilabert, E. Sanchez, J.A. Roether, D.W. Schubert, S. Virtanen, A.R. Boccaccini, Electrophoretic deposition of nanostructured-TiO2/chitosan composite coatings on stainless steel, RSC Adv. 3 (2013) 11247–11254.
[3] A.R. Boccaccini, S. Keim, R. Ma, Y. Li, I. Zhitomirsky, Electrophoretic deposition of biomaterials, J. R. Soc. Interface 7 (Suppl. 5) (2010) S581–613.
[4] A.R. Boccaccini, U. Schindler, H.G. Krueger, Ceramic coatings on carbon and metallic fibers by electrophoretic deposition, Mater. Lett. 51 (2001) 225–230.
[5] M.J. Santillan, F. Membrives, N. Quaranta, A.R. Boccaccini, Characterization of TiO2 nanoparticle suspensions for electrophoretic deposition, J. Nanopart. Res. 10 (2008) 787–793.
[6] L.Q. Wu, A.P. Gadre, H. Yi, M.J. Kastantin, G.W. Rubloff, W.E. Bentley, G.F. Payne, R. Ghodssi, Voltage-dependent assembly of the polysaccharide chitosan on to an electrode surface, Langmuir 18 (2002) 8620–8625.
[7] L.L. Hench, R.J. Splinter, W.C. Allen, T.K. Greenlee, Bonding mechanisms at the interface of ceramic prosthetic materials, J. Biomed. Mater. Res. 5 (1971) 117–141.
[8] I.D. Xynos, A.J. Edgar, L.D.K. Buttery, L.L. Hench, J.M. Polak, Ionic products of bioactive glass dissolution increase proliferation of human osteoblasts and induce insulin-like growth factor II mRNA expression and protein synthesis, Biochem. Biophys. Res. Commun. 276 (2000) 461–465.
[9] M.S. Bahniuk, H. Pirayesh, H.D. Singh, J.A. Nychka, L.D. Unsworth, Bioactive glass 45S5 powders: effect of synthesis route and resultant surface chemistry and crystallinity on protein adsorption from human plasma, Biointerphases 7 (2012) 41.
[10] J.R. Jones, Review of bioactive glass: from Hench to hybrids, Acta Biomater. 9 (2013) 4457–4486.
[11] I.D. Xynos, A.J. Edgar, L.D.K. Buttery, L.L. Hench, J.M. Polak, Gene-expression profiling of human osteoblasts following treatment with the ionic products of Bioglass® 45S5 dissolution, J. Biomed. Mater. Res. 55 (2001) 151–157.
[12] E.A. Effah Kaufmann, P. Ducheyne, I.M. Shapiro, Evaluation of osteoblast response to porous bioactive glass (45S5) substrates by RT-PCR analysis, Tissue Eng. 6 (2000) 19–28.
[13] D. Zhitomirsky, J.A. Roether, A.R. Boccaccini, I. Zhitomirsky, Electrophoretic deposition of bioactive glass/polymer composite coatings with and without HA nanoparticle inclusions for biomedical applications, J. Mater. Processing Technol. 209 (2009) 1853–1860.
[14] K. Wu, Y. Wang, I. Zhitomirsky, Electrophoretic deposition of TiO2 and composite TiO2-MnO2 films using benzoic and phenolic molecules as charging additives, J. Colloid Interface Sci. 352 (2010) 371–378.
[15] X. Pang, I. Zhitomirsky, Electrodeposition of composite hydroxyapatite-chitosan films, Mater. Chem. Phys. 94 (2005) 245–251.
[16] M. Dash, F. Chiellini, R.M. Ottenbrite, E. Chiellini, Chitosan—a versatile semi-synthetic polymer in biomedical applications, Prog. Polym. Sci. 36 (2011) 981–1014.
[17] M.N.V. Ravi Kumar, A review of chitin and chitosan applications, React. Funct. Polym. 46 (2000) 1–27.
[18] R.A.A. Muzzarelli, Chitosan composites with inorganics, morphogenetic proteins and stem cells, for bone regeneration, Carbohydr. Polym. 83 (2011) 1433–1445.
[19] M. Du, B. Guo, D. Jia, Newly emerging applications of halloysite nanotubes: a review, Polym. Int. 59 (2010) 574–575.
[20] C.Q. Kautz, P.C. Ryan, The 10 Å to 7 Å halloysite transition in a tropical soil sequence, Clay Clay Miner. 51 (2003) 252–263.
[21] S. Hillier, P.C. Ryan, Identification of halloysite (7 Å) by ethylene glycol solvation: the 'MacEwan effect', Clay Miner. 37 (2002) 487–496.
[22] G.Y. Jeong, Y. Kim, S. Chang, S.J. Kim, Clay nanotubes, Neues Jb. Mineral. Abh. 9 (2003) 421–429.
[23] E. Joussein, S. Petit, J. Churchman, B. Theng, D. Righi, B. Delvaux, Halloysite clay minerals — a review, Clay Miner. 40 (2005) 383–426.
[24] Y.P. Ye, H.B. Chen, J.S. Wu, L. Ye, High impact strength epoxy nanocomposites with natural nanotubes, Polymer 48 (2007) 6426–6433.
[25] M.L. Du, B.C. Guo, X.J. Cai, Z.X. Jia, M.X. Liu, D.M. Jia, Morphology and properties of halloysite nanotubes reinforced polypropylene nanocomposites, E-Polymers 130 (2008) 1–14.
[26] Z.F. Uang, Z.X. Jia, B.C. Guo, D.M. Jia, Structure and property of PBT/halloysite nanotube composite, China Plast Ind. 36 (2008) 29.
[27] Liu Mingxian, Jia Zhixin, Jia Demin, Zhou Changren, Recent advance in research on halloysite nanotubes-polymer nanocomposite, Prog. Polym. Sci. 39 (2014) 1498–1525.
[28] S.R. Levis, P.B. Deasy, Characterisation of halloysite for use as a microtubular drug delivery system, Int. J. Pharm. 243 (2002) 125–134.
[29] J. Forsgren, E. Jämstorp, S. Bredenberg, H. Engqvist, M.A. Stromme, A ceramic drug delivery vehicle for oral administration of highly potent opioids, J. Pharm. Sci. 99 (2010) 219–226.
[30] D. Lahiri, V. Singh, A.K. Keshri, S. Seal, A. Agarwal, Apatite formability of boron nitride nanotubes, Nanotechnology 22 (2011) 1–8.
[31] M. Viseras, C. Aguzzi, P. Cerezo, G. Cultrone, C. Viseras, Supramolecular structure of 5-aminosalycilic acid/halloysite composites, J. Microencapsul. 26 (2008) 279–286.
[32] C. Aguzzi, C. Viseras, P. Cerezo, I. Salcedo, R. Sanchez-Espejo, C. Valenzuela, Release kinetics of 5-aminosalicylic acid from halloysite, Colloids Surf. B. Biointerfaces 105 (2013) 75–80.
[33] N.G. Veerabadran, R.R. Price, Y.M. Lvov, Clay nanotubes for encapsulation and sustained release of drugs, Nano 02 (2007) 115–120.
[34] Y. Lvov, E. Abdullayev, Functional polymer–clay nanotube composites with sustained release of chemical agents, Prog. Polym. Sci. 38 (2013) 1690–1719.
[35] E. Abdullayev, Y. Lvov, Halloysite clay nanotubes as a ceramic "Skeleton" for functional biopolymer composites with sustained drug release, J. Mater. Chem. B 1 (2013) 2894–2903.
[36] I. Deen, X. Pang, I. Zhitomirsky, Electrophoretic deposition of composite chitosan–halloysite nanotube-hydroxyapatite films, Colloids Surf. A Physicochem. Eng. Asp. 410 (2012) 38–44.

[37] I. Deen, I. Zhitomirsky, Electrophoretic deposition of composite halloysite nanotube–hydroxyapatite–hyaluronic acid films, J. Alloys Compd. 586 (2013) S531–S534.
[38] D. Davies, Understanding biofilm resistance to antibacterial agents, Nat. Rev. Drug Discov. 2 (2003) 114–122.
[39] K.C. Popat, M. Eltgroth, T.J. LaTempa, C.A. Grimes, T.A. Desai, Titania nanotubes: a novel platform for drug-eluting coatings for medical implants? Small 3 (2007) 1878–1881.
[40] A. Simchi, E. Tamjid, F. Pishbin, A.R. Boccaccini, Recent progress in inorganic and composite coatings with bactericidal capability for orthopaedic applications, Nanomedicine 7 (2011) 22–39.
[41] Qi Ruiling, G. Rui, S. Mingwu, C. Xueyan, Z. Leqiang, Xu Jiajia, Yu Jianyong, S. Xiangyang, Electrospun poly(lactic-co-glycolic acid)/halloysite nanotube composite nanofibers for drug encapsulation and sustained release, J. Mater. Chem. 20 (2010) 10622–10629.
[42] Test Method for Measuring Adhesion by Tape Test; ASTM Standard D3359-B; American Society for Testing and Materials (ASTM) International: West Conshohocken, PA, USA.
[43] T. Kokubo, H. Takadama, How useful is SBF in predicting in vivo bone bioactivity? Biomaterials 27 (2006) 2907–2915.
[44] Y.M. Yang, Y.H. Zhao, X.H. Liu, F. Ding, X.S. Gu, The effect of different sterilization procedures on chitosan dried powder, J. Appl. Polym. Sci. 104 (2007) 1968–1972.
[45] V. Vergaro, E. Abdullayev, Y.M. Lvov, A. Zeitoun, R. Cingolani, R. Rinaldi, S. Leporatti, Cytocompatibility and uptake of halloysite clay nanotubes, Biomacromolecules 11 (2010) 820–826.
[46] R.R. Price, B.P. Gaber, Y. Lvov, In-vitro release characteristics of tetracycline HC1, khellin and nicotinamide adenine dineculeotide from halloysite; a cylindrical mineral, J. Microencapsul. 18 (2001) 713–722.
[47] H.M. Kelly, P.B. Deasy, E. Ziaka, N. Clafftey, Formulation and preliminary in vivo dog studies of a novel drug delivery system for the treatment of periodontitis, Int. J. Pharm. 274 (2004) 167–183.
[48] I. Zhitomirsky, A. Hashambhoy, Chitosan-mediated electrosynthesis of organic-inorganic nanocomposites, J. Mater. Process. Technol. 191 (2007) 68–72.
[49] I. Zhitomirsky, Cathodic electrophoretic deposition of ceramic and organic-ceramic materials, fundamental aspects, Adv. Colloid Interface Sci. 97 (2002) 279–317.
[50] K. Grandfield, I. Zhitomirsky, Electrophoretic deposition of composite hydroxyapatite–silica–chitosan coatings, Mater. Charact. 59 (2008) 61–67.
[51] F. Pishbin, V. Mourino, S. Flor, S. Kreppel, V. Salih, M.P. Ryan, A.R. Boccaccini, Electrophoretic deposition of gentamicin-loaded bioactive glass/chitosan composite coatings for orthopaedic implants, ACS Appl. Mater. Interfaces 6 (2014) 8796–8806.
[52] C. Paluszkiewics, E. Stodolakl, M. Blazewicz, FTIR study of montmorillonite-chitosan nanocomposite materials, Spectrochim. Acta 79 (2011) 784–788.
[53] N. Raddaha, S. Seuss, A.R. Boccaccini, Study of the electrophoretic deposition of chitosan/halloysite nanotubes/titanium dioxide composite coatings using taguchi experimental design approach, Key Eng. Mater. 654 (2015) 230–239.
[54] Y. Peng, P.D. Southon, Z. Liu, M.E.R. Green, J.M. Hook, S.J. Antill, C.J. Kepert, Functionalization of halloysite clay nanotubes by grafting with γ-aminopropyltriethoxysilane, J. Phys. Chem. C 112 (2008) 15742–15751.
[55] E. Kontonasaki, T. Zorba, L. Papadopoulou, E. Pavlidou, X. Chatzistavrou, K. Paraskevopoulos, P. Koidis, Hydroxy carbonate apatite formation on particulate bioglass in vitro as a function of time, Cryst. Res. Technol. 37 (2002) 1165–1171.
[56] L. Cordero-Arias, S. Cabanas-Polo, J. Gilabert, O.M. Goudouri, E. Sanchez, S. Virtanen, A.R. Boccaccini, Electrophoretic deposition of nanostructured TiO_2/alginate and TiO_2-bioactive glass/alginate composite coatings on stainless steel, Adv. Appl. Ceram. 113 (2014) 42–49.
[57] A. Molaei, A. Amadeh, M. Yari, M. Reza Afshar, Structure, apatite inducing ability, and corrosion behavior of chitosan/halloysitenanotube coatings prepared by electrophoretic deposition on titanium substrate, Mater. Sci. Eng. C 59 (2016) 740–747.
[58] S. Seuss, M. Lehmann, A.R. Boccaccini, Alternating current electrophoretic deposition of antibacterial bioactive glass-chitosan composite coatings, Int. J. Mol. Sci. 15 (2014) 12231–12242.
[59] K.L. Menzies, L. Jones, The impact of contact angle on the biocompatibility of biomaterials, Optom. Vis. Sci. 87 (2010) 1401–1409.
[60] J.D. Bumgardner, R. Wiser, S.H. Elder, R. Jouett, Y. Yang, J.L. Ong, Contact angle, protein adsorption and osteoblast precursor cell attachment to chitosan coatings bonded to titanium, J. Biomater. Sci. Polym. Ed. 14 (2003) 1401–1409.
[61] S. Farris, L. Introzzi, P. Biagioni, T. Holz, A. Schiraldi, L. Piergiovanni, Wetting of biopolymer coatings: contact angle kinetics and image analysis investigation, Langmuir 27 (2011) 7563–7574.
[62] O. Kylián, O. Polonskyi, J. Kratochvíl, A. Artemenko, A. Choukourov, M. Drábik, P. Solař, D. Slavínská, H. Biederman, Control of wettability of plasma polymers by application of Ti nano-clusters, Plasma Process. Polym. 9 (2012) 180–187.
[63] Li Wei, Di Yaping, Yu Shanshan, Yao Qingqing, A.R. Boccaccini, Multifunctional chitosan-45S5 bioactive glass-poly (3-hydroxybutyrate-co-3-hydroxyvalerate) microsphere composite membranes for guided tissue/bone regeneration, ACS Appl. Mater. Interfaces 7 (2015) 20845–20854.
[64] K.T. Bowers, J.C. Keller, B.A. Randolph, D.G. Wick, C.M. Michaels, Optimization of surface micromorphology for enhanced osteoblast responses in vitro, Int. J. Oral Maxillofac. Implants 7 (1992) 302–310.
[65] S. Ozawa, S. Kasugai, Evaluation of implant materials (hydroxyapatite, glass-ceramics, titanium) in rat bone marrow stromal cell culture, Biomaterials 17 (1996) 23–29.
[66] B. Gehroudi, T.R.L. Could, D.M. Brunette, Titanium coated micromachined grooves of different dimensions effect epithelial and connective tissue cells differently in vivo, J. Biomed. Mater. Res. 24 (1990) 1203–1219.
[67] B. Gehroudi, T.R.L. Could, D.M. Brunette, Effect of grooves titanium coated implant surface on epithelial cell behavior, in vitro and in vivo, J. Biomed. Mater. Res. 24 (1990) 1067–1085.
[68] D.M. Brunette, The effects of implant surface topography on the behavior of cells, Int. J. Oral Maxillofac. Implants 3 (1988) 231–246.
[69] C.M. Michaels, J.C. Keller, C.M. Stanford, M. Solursh, In vitro cell attachment of osteoblast-like cells to titanium, J. Dent. Res. 68 (special issue) (1989) 276.
[70] Q. Yao, P. Nooeaid, R. Detsch, J.A. Roether, Y. Dong, O.M. Goudouri, D.W. Schubert, A.R. Boccaccini, Bioglass®/chitosan–polycaprolactone bilayered composite scaffolds intended for osteochondral tissue engineering, J. Biomed. Mater. Res. A 102A (2014) 4510–4518.
[71] M.N. Rahaman, D.E. Day, B.S. Bal, Q. Fu, S.B. Jung, L.F. Bonewald, A.P. Tomsia, Bioactive glass in tissue engineering, Acta Biomater. 7 (2011) 2355–2373.
[72] L.C. Gerhardt, A.R. Boccaccini, Bioactive glass and glass–ceramic scaffolds for bone tissue engineering, Materials 3 (2010) 3867–3910.
[73] P. Ducheyne, Q. Qiu, Bioactive ceramics: the effect of surface reactivity on bone formation and bone cell function, Biomaterials 20 (1999) 2287–2303.
[74] H.K. Kim, J.W. Jang, C.H. Lee, Surface modification of implant materials and its effect on attachment and proliferation of bone cells, J. Mater. Sci. Mater. Med. 15 (2004) 825–830.
[75] K. Anselme, Osteoblast adhesion on biomaterials, Biomaterials 21 (2000) 667–681.
[76] K.L. Menzies, L. Jones, The impact of contact angle on the biocompatibility of biomaterials, Optom. Vis. Sci. 87 (2010) 1401–1409.
[77] J.D. Bumgardner, R. Wiser, S.H. Elder, R. Jouett, Y. Yang, J.L. Ong, Contact angle, protein adsorption and osteoblast precursor cell attachment to chitosan coatings bonded to titanium, J. Biomater. Sci. Polym. Ed. 14 (2003) 1401–1409.
[78] P.S. Gomes, M.H. Fernandes, Effect of therapeutic levels of doxycycline and minocycline in the proliferation and differentiation of human bone marrow osteoblastic cells, Oral Biol. 52 (2007) 251–259.
[79] D.O. Costa, P.D.H. Prowse, T. Chrones, S.M. Sims, D.W. Hamilton, A.S. Rizkalla, S.J. Dixon, The differential regulation of osteoblast and osteoclast activity by surface topography of hydroxyapatite coatings, Biomaterials 34 (2013) 7215–7226.
[80] S.K. Misra, T. Ansari, D. Mohn, S.P. Valappil, T.J. Brunner, W.J. Stark, I. Roy, J.C. Knowles, P.D. Sibbons, E.V. Jones, A.R. Boccaccini, V. Salih, Effect of nanoparticulate bioactive glass particles on bioactivity and cytocompatibility of poly(3-hydroxybutyrate) composites, J. R. Soc. Interface 7 (2010) 453–465.
[81] C. Kumar, Nanostructured Thin Films and Surfaces, Wily-VCH, Germany, 2010.
[82] G. Mario, G. Gabriele, Mathematical modelling and controlled drug delivery: matrix systems, Curr. Drug Deliv. 2 (2005) 97–116.
[83] J.M. Xue, M. Shi, PLGA/mesoporous silica hybrid structure for controlled drug release, J. Control. Release 98 (2004) 209–217.
[84] M. Islam, S. Masum, K. Rayhan, Z. Haque, Antibacterial activity of Crab-Chitosan against *Staphylococcus aureus* and *Escherichia coli*, J. Adv. Sci. Res. 2 (2011) 63–66.
[85] S. Hu, J. Chang, M. Liu, C. Ning, Study on antibacterial effect of 45S5 Bioglass, J. Mater. Sci. Mater. Med. 20 (2009) 281–286.